Li, XP; Cai, Y; Yang, HY; Lahteenmaki, A; Tornikoski, M; Tammi, J; Suutarinen, S; Yang, Hai-Tao; Luo, YH; Wang, LS

Quasi-periodic behaviour in the radio and gamma-ray light curves of blazar PKS 1510-089

Published in:
Monthly Notices of the Royal Astronomical Society

DOI:
10.1093/mnras/stad008

Published: 01/03/2023

Document Version
Publisher's PDF, also known as Version of record

Please cite the original version:
Li, XP., Cai, Y., Yang, HY., Lahteenmaki, A., Tornikoski, M., Tammi, J., Suutarinen, S., Yang, H.-T., Luo, YH., & Wang, LS. (2023). Quasi-periodic behaviour in the radio and gamma-ray light curves of blazar PKS 1510-089. *Monthly Notices of the Royal Astronomical Society*, *519*(4), 4893-4901. https://doi.org/10.1093/mnras/stad008

Monthly Notices of the ROYAL ASTRONOMICAL SOCIETY

MNRAS **519,** 4893–4901 (2023) https://doi.org/10.1093/mnras/stad008
Advance Access publication 2023 January 5

Quasi-periodic behaviour in the radio and γ-ray light curves of blazar PKS 1510−089

Xiao-Pan Li ,[1]★ Yan Cai,[1] Hai-Yan Yang,[1] Anne Lähteenmäki,[2,3] Merja Tornikoski,[2] Joni Tammi,[2] Sofia Suutarinen,[2,4] Hai-Tao Yang,[1] Yu-Hui Luo[1,5] and Li-Sha Wang[1]

[1]*College of Physics and Information Engineering, Zhaotong University, Zhaotong 657000, China*
[2]*Metsähovi Radio Observatory, Aalto University, Metsähovintie 114, FI-02540 Kylmälä, Finland*
[3]*Department of Electronics and Nanoengineering, Aalto University, PO Box 15500, FI-00076 Espoo, Finland*
[4]*Finnish Centre for Astronomy with ESO (FINCA), University of Turku, Vesilinnantie 5, FI-20014 Turku, Finland*
[5]*Faculty of Civil Engineering and Mechanics/Faculty of Science, Kunming University of Science and Technology, Kunming 650500, China*

Accepted 2022 December 29. Received 2022 December 6; in original form 2022 October 11

ABSTRACT

We explore the possible quasi-periodic oscillations (QPOs) of the blazar PKS 1510−089, utilizing the ∼38-yr Metsähovi flux density observations at 37 GHz and over 10-yr *Fermi* Large Area Telescope observations in the 0.1–300 GeV energy range. Both the flux distributions of the radio and γ-ray light curves suggest a lognormal distribution, and power spectral densities of both light curves can be well represented by a bending power-law model. Comparing the results from the weighted wavelet Z-transform and Lomb–Scargle periodogram approaches, a quasi-period of 1330 ± 55 d at a 99.80 per cent ($>3\sigma$) significance against the red noise background is observed in the radio light curve, whereas no similar modulation is seen in the γ-ray light curve. We briefly discuss the research actuality of blazar QPO phenomena and explain the observed radio QPO as the result of Keplerian motion in a supermassive binary black hole system and periodic modulation induced by the Lense–Thirring precession of the innermost portions of the accretion disc.

Key words: galaxies: active – BL Lacertae objects: general – BL Lacertae objects: individual: PKS 1510−089.

1 INTRODUCTION

Blazars represent the most active subclass of active galactic nuclei (AGNs) powered by accretion on to supermassive black holes (SMBHs) in galaxies. The rich phenomenology of blazars, such as violent and rapid flux variability ranging from radio wavelength to TeV γ-ray energies, high and variable polarization at radio and optical wavelength, strongly beamed non-thermal radiation dominated by relativistic jets along the line of sight, superluminal jet speeds, usually core-dominated radio structures, etc., has made it the ideal source for extragalactic astronomy (e.g. Urry & Padovani 1995). The emissions from blazars are characterized by variabilities on different time-scales and can provide information about the nature of blazars. In general, blazars show stochastic and aperiodic variations in their brightness (e.g. Vaughan 2005; Sobolewska et al. 2014; Vaughan et al. 2016; Kushwaha et al. 2017; Zheng et al. 2017; Goyal et al. 2018; Zhou et al. 2021). Using a stochastic model to fit the time series, Vaughan et al. (2016) discovered that when the claimed period lasted only a few cycles ($\lesssim$5 cycles), periodic or mixed periodic/stochastic signals could not be distinguished from stochastic processes. A search for periodic variations in *R*-band monitoring data of 31 blazars extending over 10 yr is consistent with the expected false alarm rate (Nilsson et al. 2018). Recently, Covino, Sandrinelli & Treves (2019) and Ait Benkhali et al. (2020) analysed a sample of 10 and 6 blazars, respectively, to search for periodicity in *Fermi* Large Area Telescope (*Fermi*-LAT) γ-ray observations spanning ∼10 yr. However, no strong evidence of periodicity in their sample was found.

However, since periodic flux modulation can constrain the physical process of blazar variation and optimize the scheduling of multiwavelength observations, the search and interpretation of periodic signals in light curves is of great interest. It is increasingly clear that blazar light curves related to their variabilities appear to show an intriguing phenomenon called quasi-periodic oscillations (QPOs), which have been found in all observable energy bands and over a wide range of time-scales from minutes to years (e.g. Gupta, Srivastava & Wiita 2009; Ackermann et al. 2015; Bhatta et al. 2016; Sandrinelli et al. 2016; Bhatta 2017, 2021; Caproni et al. 2017; Sobacchi, Sormani & Stamerra 2017; Yang et al. 2021a; Zhang et al. 2021; Roy et al. 2022, and references therein). Over the past few decades, a large collective effort to research the periodic or quasi-periodic properties of multiwavelength light curves has promoted research on the nature of blazars, e.g. the origin and inner structure of the jets (e.g. Mohan & Mangalam 2015; Sobacchi et al. 2017; Zhou et al. 2018; Otero-Santos et al. 2020; Sarkar et al. 2020, 2021), dynamical, thermal, and viscous processes occurring in accretion discs (e.g. Gupta et al. 2009; Lachowicz et al. 2009; Wang et al. 2014; Kaur et al. 2017; Liska et al. 2018), constraints on disc–jet connection (e.g. An et al. 2013; King et al. 2013; Sandrinelli et al. 2016), and other extrinsic efforts like jet precession due to a nearby massive object or supermassive binary black hole (SMBBH) systems (e.g. Ackermann et al. 2015; Graham et al. 2015; Mohan & Mangalam 2015; Sandrinelli et al.

★ E-mail: lxpzrc@163.com

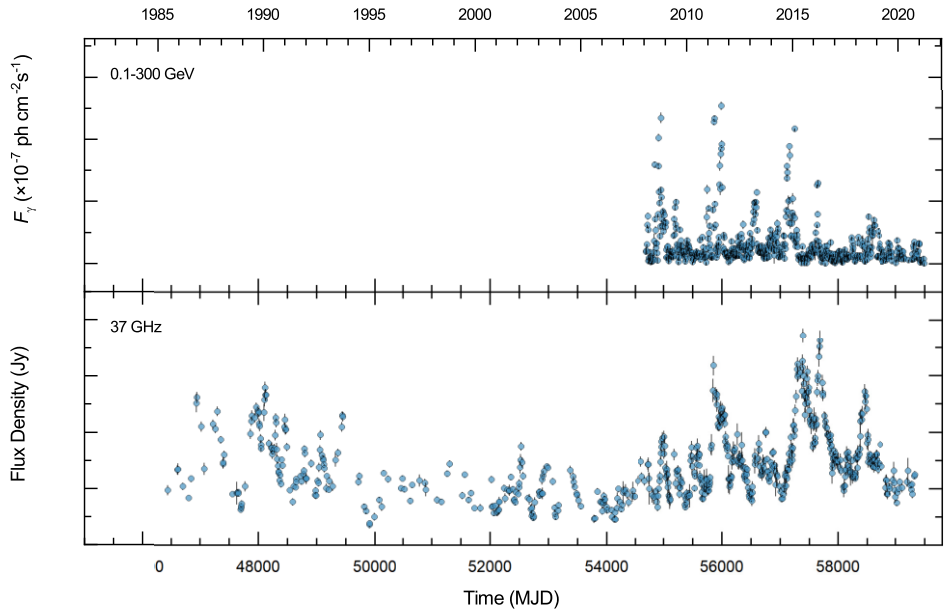

Figure 1. Weekly binned light curves of the blazar PKS 1510−089. *Top panel*: *Fermi*-LAT γ-ray light curve at 0.1–300 GeV from 2008 August 22 to 2021 October 1, spanning ∼13 yr, with test statistic >25. *Bottom panel*: Metsähovi light curve at 37 GHz from 1983 April 16 to 2021 April 30, spanning ∼38 yr.

2016; Caproni et al. 2017; Li et al. 2017, 2018, 2021b; Sobacchi et al. 2017; Zhang et al. 2017a; Ren et al. 2021). Despite the growing evidence for the existence of the QPOs in blazar variability, the QPO driving mechanism remains controversial. An adequate solution to this problem would be to search for and explain the QPO from multiwavelength variabilities related to the accretion discs and/or the jets.

The blazar PKS 1510−089 is among the few blazars whose multiwavelength light curves are claimed to be periodic. It is a bright and highly variable blazar at a redshift (z) of 0.361 (Tanner et al. 1996) discovered in the MeV–GeV band by the *Energetic Gamma Ray Experiment Telescope* (Hartman et al. 1999). It was classified as a flat-spectrum radio quasar (FSRQ), one subclass of blazars, due to the presence of strong and broad emission lines produced by gas in the broad-line region (BLR). As one of only a few FSRQs detected in very high energy (VHE; >100 GeV) γ-ray band, PKS 1510−089 shows interesting VHE flaring activities that are hard to explain within the current models of FSRQs and are probably produced outside of the BLR, and even far down in the jets (e.g. Aleksić et al. 2014; Costamante et al. 2018; MAGIC Collaboration 2018; Zacharias et al. 2019; H.E.S.S. Collaboration 2021). Similarly to many other FSRQs, PKS 1510−089 is strongly variable from the radio to γ-rays. In the optical R band, Xie et al. (2004) reported a large-amplitude variation of 1.35 mag with a short time-scale of 89 min. The rapid and high-amplitude γ-ray flares with the flux doubling time-scales less than 1 h had been identified by Saito et al. (2013). This source is also characterized by quiescent periods followed by large-amplitude outbursts that consist of several flares on time-scales of several days to months. Interestingly, multiwavelength emissions show that the γ-ray flares were usually accompanied by large radio and optical outbursts (e.g. Marscher et al. 2010; Orienti et al. 2013; Beaklini, Dominici & Abraham 2017), although sometimes this correlation could be hidden due to the existence of observational gaps (e.g. Bonning et al. 2012; Rajput, Stalin & Sahayanathan 2020).

The continuing operations of the *Fermi*-LAT and Metsähovi Radio Observatory program continually provide sensitive γ-ray data over the energy range of ∼100 MeV to 300 GeV and radio data at 22 and 37 GHz, which makes it possible to search for QPOs on long-term time-scales. In this work, we describe the *Fermi*-LAT and Metsähovi observations of PKS 1510−089 in Section 2, and present the results of searching for QPOs by different approaches in Section 3. We finally present our discussion and conclusions in Section 4.

2 OBSERVATIONS

We generated the weekly binned γ-ray light curve from the Pass 8 LAT data, following the standard procedure of the binned likelihood analysis provided in the *Fermi* Science Support Center (FSSC).[1] The analysis was done using the *Fermi* Science Tools software version v11r5p3 with the instrument response functions 'P8R3_SOURCE_V3' for SOURCE events (evclass = 128, evtype = 3). The region of interest (ROI) of 15° radius centred on PKS 1510−089, maximum zenith angle of 90°, and good time intervals with the expression '(DATA_QUAL>0)&&(LAT_CONFIG = = 1)' were adopted. The diffuse galactic and extragalactic background emissions were modelled using two files: *gll_iem_v07.fits* and *iso_P8R3_SOURCE_V3_v1.txt*. The source model XML file was created using the script *make4FGLxml.py*[2] based on the *Fermi* Large Telescope Fourth Source Catalog (Abdollahi et al. 2020). The normalizations and spectral parameters from all sources within 5° centred at the centre of ROI were set free. We performed the binned likelihood analysis (see e.g. Abdo et al. 2009) using the tool *gtlike* to obtain the integrated flux values and the significance for each weekly time bin. Photon flux with test statistic >25 (∼5σ; see Mattox et al. 1996) covering the interval from 2008 August 22 (MJD 54700) to 2021 October 1 (MJD 59488) is considered in the following analyses and is reported in the top panel of Fig. 1.

[1] https://fermi.gsfc.nasa.gov/ssc/data/analysis/scitools/binned_likelihood_tutorial.html
[2] https://fermi.gsfc.nasa.gov/ssc/data/analysis/user/make4FGLxml.py

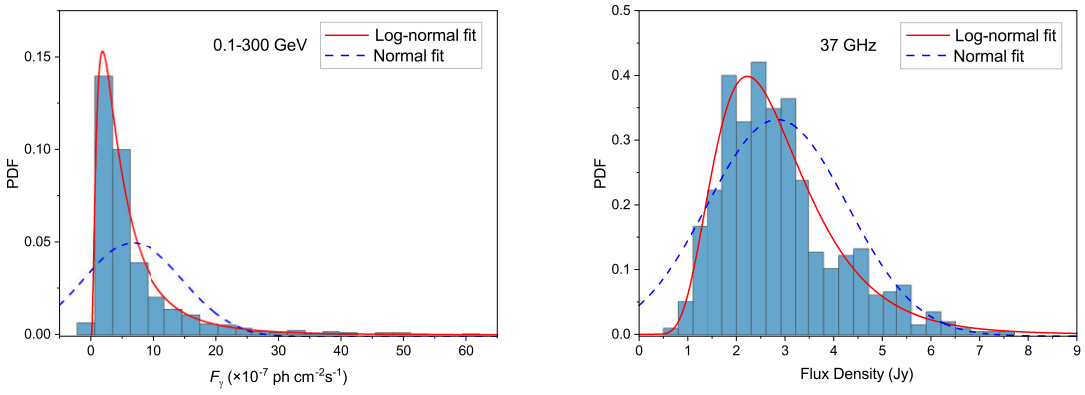

Figure 2. *Left-hand panel*: flux histogram of the γ-ray observations with 25 bins. The red solid line and blue dashed line show the lognormal and normal PDF fits to the observations, respectively. *Right-hand panel*: same as left-hand panel, but for the radio fluxes.

The 37-GHz observations were carried out on the 14-m-diameter radio telescope, which is a radome-enclosed paraboloid antenna located at Metsähovi Radio Observatory[3] of Aalto University, Finland. Metsähovi observations had been widely used in multiwavelength study of AGNs, including individual blazars, such as PKS 1510−089, S5 0716+714, 3C 454.3, and selected samples (e.g. Hovatta et al. 2007; Aleksić et al. 2014; Ramakrishnan et al. 2015; Lähteenmäki et al. 2018; MAGIC Collaboration 2018; Sarkar et al. 2019; Goyal et al. 2022). Radio observations with a signal-to-noise ratio >4 were weekly binned to smooth short-term fluctuations of the light curves. The error estimate in the flux density includes the contribution from the measurement root mean square (rms) and the uncertainty of the absolute calibration. At 37 GHz, this telescope has a detection limit of ∼0.2 Jy. A detailed description of the telescope, observation methods, and analysis procedure can be found in Teraesranta et al. (1998). We then present the ∼38-yr weekly averaged 37-GHz light curve, from 1983 April 16 to 2021 April 30 (MJD 45440–59335), in the bottom panel of Fig. 1.

3 RESULTS

3.1 Fractional variability and flux distribution

Fig. 1 already illustrates that both the γ-ray and radio emissions are highly variable, with flaring events typically separated by several months or years. We further calculated the fractional variability amplitude $F_{\rm var}$ (Edelson et al. 2002) to quantify the intrinsic variability of the light curves. $F_{\rm var}$ and its uncertainty are presented in the form of

$$F_{\rm var} = \sqrt{\frac{S^2 - \langle\sigma_{\rm err}^2\rangle}{\langle f\rangle^2}}, \tag{1}$$

for which the uncertainty is estimated by

$$\sigma_{F_{\rm var}} = \frac{1}{F_{\rm var}}\sqrt{\frac{1}{2N}}\frac{S^2}{\langle f\rangle^2}, \tag{2}$$

where S^2 is the sample variance, $\langle\sigma_{\rm err}^2\rangle$ is the mean square uncertainty, and $\langle f\rangle$ is the mean value of the measurements. $F_{\rm var}$ at γ-ray energies was measured to be 1.17 ± 0.03, and that in the radio band is 0.41 ± 0.01, which indicates that the flux variability at γ-ray energies varies more violently than in the radio band. This is probably due to the shorter cooling time for higher energy particles, which leads to faster variabilities and more variations at higher energies (e.g. Massaro et al. 2004; Zheng et al. 2017; Roy et al. 2019).

Flux distribution belongs to one of the most important properties of a light curve, which is usually used to explore the origin and nature of the variability in blazars. Probability density function (PDF) of the flux distribution can be estimated. In Fig. 2, the distribution of the binned γ-ray photon fluxes and radio fluxes of PKS 1510−089 is presented in histograms with 25 bins. We then used the lognormal and normal functions to fit the PDFs, respectively. The lognormal model for PDF can be expressed as

$$\mathrm{PDF}_{\rm lognormal}(x) = \frac{1}{\sqrt{2\pi}x\sigma}\exp\left[-\frac{(\ln x - \mu)^2}{2\sigma^2}\right], \tag{3}$$

where σ and μ represent the scale parameter and the mean flux location of the PDF, respectively. Similarly, the normal PDF has the form of

$$\mathrm{PDF}_{\rm normal}(x) = \frac{1}{\sqrt{2\pi}\sigma}\exp\left[-\frac{(x - \mu)^2}{2\sigma^2}\right], \tag{4}$$

where σ and μ represent the standard deviation and the mean value of the PDF, respectively. The lognormal and normal PDFs for the γ-ray and radio light curves are overplotted in Fig. 2, in which both γ-ray and radio flux distributions are asymmetric with a heavy tail extending towards higher flux level. Table 1 lists the best-fitting parameters for the lognormal and normal distributions. It can be found that the scaled lognormal model provides good apparent fits to both histograms of the γ-ray and radio data, according to the reduced χ^2 obtained for these two models. In blazars, lognormal distribution can be considered to be produced in non-linear multiplicative processes, such as instabilities at the disc and the jet, disc–jet connection processes, variable radiation by the up-scattered photons, extrinsic geometrical and projection effects, or coupling of the above processes (e.g. Uttley, McHardy & Vaughan 2005; Shah et al. 2018; Zheng et al. 2019; Bhatta & Dhital 2020). The fitted parameters σ and μ of the lognormal PDF were adopted as inputs in the light-curve simulations (see Sections 3.2 and 3.3).

3.2 Power spectral density analysis

Power spectral density (PSD) analysis is a reliable and frequently used technique to characterize AGN variability. Periodic flux modulations persisting for a few cycles may sometimes be seen in blazar light curves that are mostly dominated by power-law-type noise, particularly in the low-frequency range (e.g. Press 1978; Vaughan

[3] http://www.metsahovi.fi/opendata/

Table 1. The best-fitting parameters and the corresponding reduced χ^2 of the lognormal and normal PDF fitting to the histogram of the *Fermi*-LAT and radio light curves. For the normal PDF fitting, parameters μ and σ are in units of flux, whereas for the lognormal, μ is in units of the natural log of flux.

Light curves	Lognormal			Normal		
	μ	σ	χ^2	μ	σ	χ^2
Fermi-LAT	1.46 ± 0.07	0.93 ± 0.05	13.85	6.73 ± 0.63	7.91 ± 0.42	206.55
Radio	0.97 ± 0.03	0.41 ± 0.02	46.62	2.87 ± 0.09	1.20 ± 0.06	69.90

et al. 2016; Bhatta 2017; Covino et al. 2019; Li et al. 2021b). In order to determine the intrinsic PSD of each light curve against the power-law-type noise background, we applied the power spectrum response (PSRESP) method (Uttley, McHardy & Papadakis 2002), which is a Monte Carlo-type approach and has been widely used to characterize the PSD of AGN periodogram (e.g. Chatterjee et al. 2008; Max-Moerbeck et al. 2014; Bhatta et al. 2016; Ait Benkhali et al. 2020; Bhatta 2021; Goyal et al. 2022). The logarithmically binned source periodogram is fitted with various model PSDs with varying parameters to determine which one has the greatest probability that the source PSD can be best represented. The method uses a large number of simulated light curves that have similar statistical properties to the original light curves, such as mean, standard deviation, sampling pattern, and observation duration, to provide an estimate for the goodness of fit of model PSDs.

The PSD $P(\nu_k)$ with the fractional rms-squared normalization for given time series $f(t_i)$ of duration T sampled at N instances t_i is expressed as

$$P(\nu_k) = \frac{2T}{\mu^2 N^2} \left| \sum_{i=1}^{N} f(t_i) e^{-i2\pi\nu_k t_i} \right|^2, \tag{5}$$

with $\nu_k = k/T$, $k = 1,..., N/2$, where the maximum frequency is the Nyquist frequency $\nu_{\rm Nyq} = N/2T$ and μ is the mean of the time series. With this normalization, the total integrated power of the periodogram is almost equal to the time series' variance. In order to reduce the dispersion of the periodogram and facilitate PSD model fitting, the periodogram was usually binned using the appropriate frequency bins.

For the underlying power spectrum, we simulate PSDs with a simple power-law model of the form $P(\nu) \propto \nu^{-\beta} + C_{\rm noise}$, where ν and β represent temporal frequency and spectral index, respectively, and $C_{\rm noise}$ is a constant noise floor level from measurement uncertainties that is fixed at the Poisson noise level for the light curve. Due to the logarithmic binning of the power spectra and the difficulty of subtracting constants in a linear space, we first estimated $C_{\rm noise}$ using (e.g. Goyal et al. 2022)

$$C_{\rm noise} = \frac{2T}{\mu^2 N} \overline{\sigma_{\rm err}^2}, \tag{6}$$

where $\sigma_{\rm err}$ represents the flux uncertainties. A series of trial spectral indices, usually in a range of 0.5–3.0 with a step of 0.05 or 0.1, are used to test the goodness of fit. We then simulated 10 000 light curves for each trial spectral index using the Emmanoulopoulos, McHardy & Papadakis (2013) algorithm, which represents an improvement over the procedure of Timmer & Koenig (1995). The Emmanoulopoulos algorithm can reproduce light curves that preserve both the PDF and the power spectral shape of a real light curve or a theoretical model. In this work, the PYTHON implementation[4] provided by Connolly (2015) was employed.

Subsequently, the statistical properties of the observed light curve were applied to the simulated light curves via resampling and interpolation, and then the PSD of the observed light curve $[P_{\rm obs}(\nu)]$ and the PSDs of each simulated light curve $[P_{{\rm sim},i}(\nu)]$ were calculated using the same binning pattern and procedure. The χ^2-like statistic was calculated for the observed light curve and each of the simulated light curves as follows:

$$\chi^2_{\rm obs} = \sum_{\nu=\nu_{\rm min}}^{\nu_{\rm max}} \frac{\left[P_{\rm obs}(\nu) - \overline{P_{\rm sim}(\nu)}\right]^2}{\overline{\Delta P_{\rm sim}(\nu)}^2}, \tag{7}$$

$$\chi^2_{{\rm dist},i} = \sum_{\nu=\nu_{\rm min}}^{\nu_{\rm max}} \frac{\left[P_{{\rm sim},i}(\nu) - \overline{P_{\rm sim}(\nu)}\right]^2}{\overline{\Delta P_{\rm sim}(\nu)}^2}, \tag{8}$$

where $\overline{P_{\rm sim}(\nu)}$ and $\overline{\Delta P_{\rm sim}(\nu)}$ are the mean periodogram and standard deviation of all the simulated periodograms, respectively; i runs over the number of simulated light curves for a trail spectral index β. $\chi^2_{\rm dist}$ for each simulated PSD over the log-binned frequencies was calculated. The goodness of fit for a given model (simple power-law model, here) can be evaluated by the ratio of the number of $\chi^2_{\rm dist}$s greater than $\chi^2_{\rm obs}$ to the total number of $\chi^2_{\rm dist}$s distribution, which gives the probabilities of a model being accepted. We then calculated the ratios using various trial spectral indices to determine the best-fitting power-law spectral index that gives the highest probability and represents the shape of the intrinsic PSD.

We applied the PSRESP method with a range of trial spectral indices of 0.5–2.0 in steps of 0.1 for the *Fermi*-LAT γ-ray light curve, and present the resulting PSD analyses in the left-hand panel of Fig. 3. The fitted power-law model shown as red circles, corresponding to the binned mean periodogram, was derived from 10 000 simulated light curves using the best-fitting power-law spectral index, where the errors on the best-fitting indices are the standard deviations of the simulated periodograms from the averages. In the panel, the grey line represents the unbinned source periodogram, which upon binning gives the blue points. The corresponding probability distribution over the trial spectral indices is shown in the inset of this panel. The best-fitting spectral index for the source PSD was estimated to be 1.2 ± 0.2 with the highest probability of 0.33, where the uncertainty was derived from the half-width at half-maximum (HWHM) of the Gaussian fit for the power-law index probability distribution. During the analysis, the Poisson noise level associated with the flux uncertainties was fixed to 0.15 (in power density unit) using equation (6).

Using the same procedure, the best-fitting spectral index of 1.7 ± 0.2 for the radio light curve was obtained from the probability distribution at the highest probability of 0.53. We scanned a range of trial spectral indices β from 1.0 to 2.5 with a step of 0.1 for

[4] https://github.com/samconnolly/DELightcurveSimulation

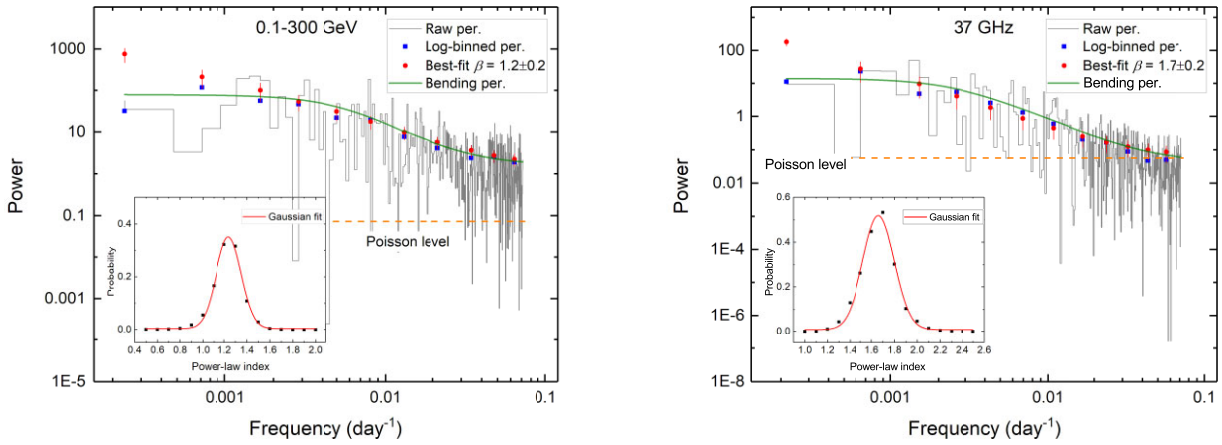

Figure 3. *Left-hand panel:* the resulting PSD analysis for the *Fermi*-LAT γ-ray light curve of PKS 1510−089, derived using the bending power-law model and the PSRESP method with a simple power-law model. Grey line, blue squares, and red circles represent the source periodogram, the corresponding logarithmically binned source periodogram, and the fitted simple power-law model, respectively. The dashed horizontal line indicates the Poisson noise level. The inset depicts the probability distribution of the trial power-law indices obtained from the PSRESP method and the corresponding Gaussian fit shown in red solid line, from which the spectral index of $\beta = 1.2 \pm 0.2$ can be derived from the simple power-law model fit. Green solid line superimposed on the periodogram shows the best-fitting bending power-law PSD whose validity was checked by means of the reduced χ^2, AIC test, and F-test. *Right-hand panel:* same as left-hand panel, but for the radio light curve. Following PSRESP, the best-fitting spectral index was estimated to be 1.7 ± 0.2 in a simple power-law model.

the simple power-law model and fixed the Poisson noise level to be 0.056. The obtained results using the PSRESP method are shown in the right-hand panel of Fig. 3. Besides, both the best-fitting spectral indices and the corresponding highest probabilities for the γ-ray and radio light curves are generally consistent with the value reported in Goyal et al. (2022), in spite of the difference in the time duration and binning pattern of the input light curves.

However, it can be seen that a pure power-law model could not describe the PSDs well at low and high frequencies simultaneously (see Fig. 3). To improve the fit, we further fit the PSDs of the light curves with a bending power-law model: $P(f) = Af^{-\alpha}/[1 + (f/f_{\rm bend})^{\beta-\alpha}] + C$, where A, α, β, $f_{\rm bend}$, and C are the normalization, low-frequency slope, high-frequency slope, bend frequency, and Poisson noise level corresponding to the power, respectively. For this model, A, C, and $f_{\rm bend}$ are all non-negative, and C is fixed to $C_{\rm noise}$ using equation (6). The fit is obtained by finding the parameters of maximum likelihood using a Basin–Hopping algorithm and a Nelder–Mead minimization algorithm provided by the PYTHON package SCIPY (Virtanen et al. 2020). The corresponding fitted values for γ-ray light curve are $A = 0.001 \pm 0.001$, $\alpha = 2.11 \pm 0.81$, $\beta = 0.0001 \pm 0.0001$, and $f_{\rm bend} = 0.0049 \pm 0.0023$, and for radio light curve are $A = 0.001 \pm 0.001$, $\alpha = 2.01 \pm 0.49$, $\beta = 0.001 \pm 0.001$, and $f_{\rm bend} = 0.0025 \pm 0.001$, respectively. The reduced χ^2 values of the PSD fits decrease from 10.72 (simple power law) to 8.57 (bending power law) for the radio light curve, and from 561.55 to 467.24 for the γ-ray light curve, respectively.

We also performed an Akaike's information criterion (AIC; Akaike 1974) test and an F-test to evaluate the significance of the fit improvement. The AIC test measures the quality of a fit of a statistical model. The preferred model is that the one with the minimum AIC value. For the γ-ray PSD fits, we found the bending power-law model with an AIC value of 1850.01 to be more consistent with the source PSD than the simple power-law model with an AIC value of 1903.21, and similarly, for the radio PSD fit, the AIC value of bending power-law model (705.00) is lower than that of the simple power-law model (784.76). The F-tests also indicate that the fit with a bending power-law model is statistically preferred over a simple power-law model, i.e. with an F-statistic of 21.05 and a null hypothesis probability $<10^{-6}$ for the γ-ray PSD fits, and an F-statistic of 30.58 and a null hypothesis probability $<10^{-6}$ for the radio PSD fits. Therefore, the goodness of the fit statistically improved when applying a bending power-law model to the PSD fits of γ-ray and radio light curves. We also present the best-fitting bending power-law PSDs in Fig. 4, shown as green solid lines.

3.3 Searching for periodicity

The weighted wavelet Z-transform (WWZ; Foster 1996) method was employed to search for possible QPOs in the γ-ray and radio light curves, which is a powerful and widely used tool to analyse non-uniform astronomical data by capturing frequency and time information simultaneously in a contour plot. If a periodic signal is non-persistent, WWZ can show its evolution with time according to the changes of the WWZ power. More details about the WWZ technique can be found in many previous works, such as Foster (1996), An et al. (2013), Bhatta et al. (2016), Sarkar et al. (2020), Li et al. (2021b), and Roy et al. (2022).

The resulting WWZ analysis is represented in Fig. 4. The left-hand panel shows the colour-scaled WWZ power spectrum for the whole *Fermi*-LAT light curve, in which possible periodic signals mainly fluctuate at about 300, 600, and 1200 d. The time-averaged WWZ power spectrum that averages WWZ power spectrum at frequencies along time provides an intuitive way to determine and locate the periodic signal while discarding its evolution. Obviously, the time-averaged WWZ spectrum as a function of frequency/period gives the strength of the signal at each frequency/period, from which distinct peaks with high WWZ powers can be considered as candidate QPOs. Then, an obvious periodicity of about 320 d, and possible periodic signals of about 620 and 1200 d corresponding to broad power peaks, can be obtained from the time-averaged WWZ power spectrum (red solid line) as shown in the right-hand panel of Fig. 4.

In order to compare and contrast the preliminary results derived from the WWZ power spectrum, another widely used method named Lomb–Scargle periodogram (LSP; Lomb 1976; Scargle 1982) has been employed in this work. Actually, these two methods have been combined quite frequently to examine the existence of the QPO in

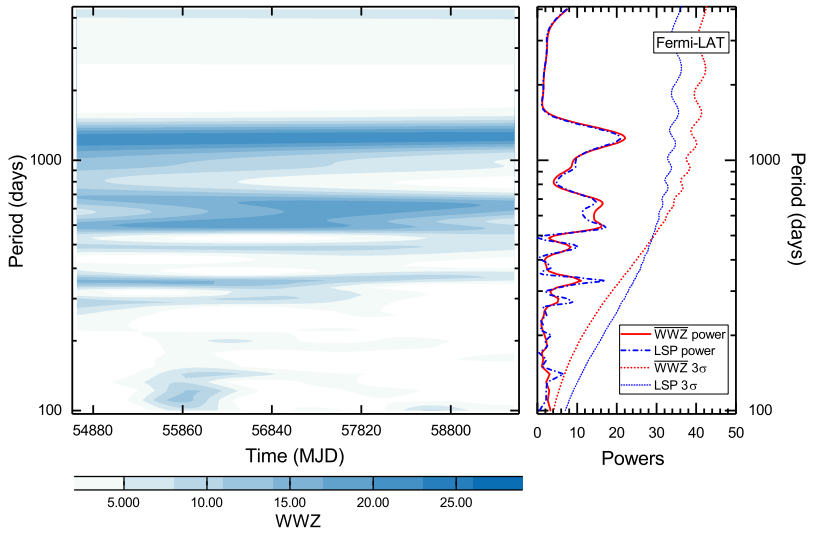

Figure 4. Periodicity analysis and significance estimation for the whole γ-ray light curve spanning ∼13 yr. *Left-hand panel*: the colour contour of the WWZ power spectrum for the *Fermi*-LAT light curve. *Right-hand panel*: the red curve and red dotted curve represent the time-averaged WWZ power spectrum and the corresponding 3σ confidence level, respectively; the blue dash–dotted curve and blue dotted curve represent the LSP spectrum and the corresponding 3σ confidence level, respectively.

blazar light curves in the last few years (e.g. Bhatta et al. 2016; Bhatta 2017; Zhang et al. 2017a,b; Zhou et al. 2018; Gupta et al. 2019; Otero-Santos et al. 2020; Li et al. 2021b; Sarkar et al. 2021; Tripathi et al. 2021; Roy et al. 2022), due to the advantages of WWZ and LSP approaches in both the time and spectral domains. The LSP power calculated for the whole *Fermi*-LAT light curve is shown as a blue dash–dotted line in the right-hand panel, which is conformable to the results obtained through the WWZ method.

Meanwhile, Fig. 5 shows the periodicity analysis for the 38-yr radio light curve. As shown in the left-hand panel, considerable WWZ power centred around 1300 d fluctuated in the middle and back half of the observations, which has been verified by the time-averaged WWZ power spectrum and the LSP power spectrum represented in the right-hand panel of Fig. 5.

Next, with the parameters of lognormal PDF fitting to the observations (see Section 3.1) and the best-fitting bending power-law model of the PSD (see Section 3.2), we simulated a total of 2×10^6 light curves to establish the red noise background for the radio and γ-ray light curves using the Emmanoulopoulos algorithm (Emmanoulopoulos et al. 2013). The artificial light curves were re-sampled to match the PDF, PSD, and statistical properties of the observed light curves. The same procedure was applied to each simulated light curve, and a series of LSP and time-averaged WWZ power spectrum can be obtained. Then, the LSP and WWZ confidence levels were established from the simulated LSP and WWZ periodograms by using the percentiles of the power at each frequency/period, respectively. In this work, a significant QPO is considered as one whose LSP power peak and time-averaged WWZ power peak are simultaneously above the corresponding 3σ LSP and WWZ confidence levels. In Figs 4 and 5, the 3σ LSP and WWZ confidence curves are superimposed on the corresponding periodograms as blue dotted and red dotted lines, respectively.

In the left-hand panel of Fig. 4, LSP and WWZ power peaks centred at about 320, 620, and 1200 d did not reach the 3σ LSP and WWZ confidence levels simultaneously. According to the confidence criterion mentioned earlier, the confidence of these possible QPOs is not significant enough. In the right-hand panel of Fig. 5 evaluated for the radio light curve, the possible QPO with high LSP and WWZ power amplitudes at 1330 ± 55 d stayed above the 3σ LSP and WWZ confidence levels, respectively. If we averaged the LSP and WWZ confidence levels at this periodicity, a confidence level of 99.80 per cent can be derived. Nevertheless, this possible QPO signal lasted for ∼10 cycles within ∼38 yr generally agrees with the WWZ colour contour. Our analysis estimated the periodicity value and uncertainties by the peak position and HWHM of the Gaussian function that fitted the WWZ power peak.

4 DISCUSSION AND CONCLUSIONS

We present time series analyses of the ∼38-yr long-term radio light curve of the FSRQ PKS 1510−089 and the ∼13-yr γ-ray observations of this source. The data were observed at Metsähovi Radio Observatory 13.7-m telescope at 37 GHz and at LAT onboard the *Fermi* Gamma-ray Space Telescope in 0.1–300 GeV, respectively. Using the LSP, WWZ methods, and the extensive Monte Carlo simulations, we observed a strong QPO signal of 1330 ± 55 d at a significance of 99.80 per cent ($>3\sigma$) over the underlying red noise processes in the radio light curve. However, no similar periodic pattern was found in the γ-ray light curve, revealing some inconsistency between γ-ray and radio emissions.

Blazar variability is usually considered to be driven by stochastic processes (e.g. Vaughan et al. 2016; Caproni et al. 2017; Ryan et al. 2019). A brief review and further references of random time series in astronomy are presented in Vaughan (2012). Stochastic process models have been applied to the optical variability of blazars that could be associated with the thermal instability of the accretion disc (e.g. Kelly, Bechtold & Siemiginowska 2009; Moreno et al. 2019; Burke et al. 2021). Moreover, γ-ray variability properties of blazars were characterized by stochastic process methods, e.g. continuous-time autoregressive moving average (e.g. Kelly et al. 2014; Ryan et al. 2019), *celerite* (e.g. Foreman-Mackey et al. 2017), and damped random-walk model (e.g. Sobolewska et al. 2014; Covino et al. 2020). The significance of QPO candidates has also been examined with stochastic process methods. By means of Gaussian processes, Covino et al. (2020) reassessed the significance of proposed periodicities, and found rather solid evidence of ∼2.2-yr QPO for PG 1553+113 in

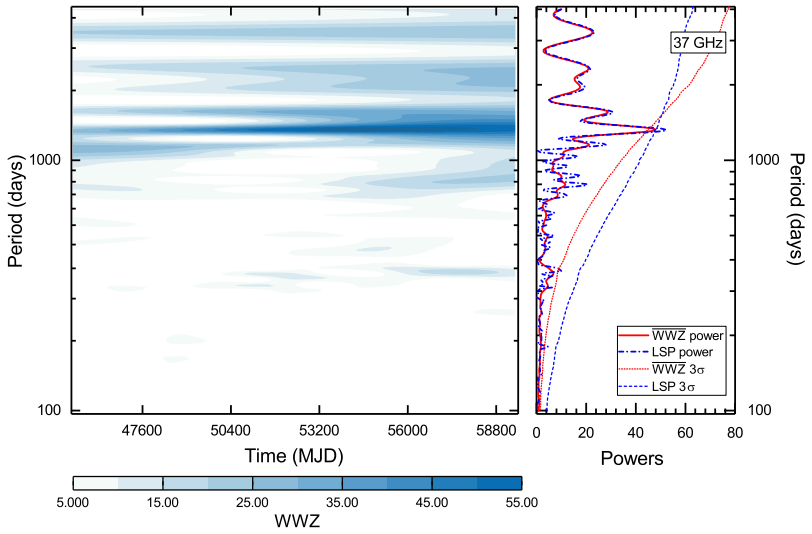

Figure 5. Same as Fig. 4, but for the radio light curve spanning ∼38 yr.

γ-ray and optical light curves. Based on the results of WWZ, LSP, and REDFIT methods, and the Gaussian process model *celerite*, a γ-ray QPO signal of ∼1.1 yr at ∼5σ confidence level was found in AGN PKS 0521−36 (Zhang et al. 2021). After characterizing the γ-ray variability in a sample of 27 blazars with the stochastic process methods, Yang et al. (2021b) found that a possible QPO feature appeared in PKS 0537−441 and PG 1553+113, and γ-ray variabilities of other sources were essentially Gaussian processes.

Recently, several works have been applied to search for QPO in homogeneous light curves of a large sample of AGNs, which is an improvement on the study of quasi-periodic behaviour: not just more QPO candidates can be detected, but the false positive rate (Vaughan et al. 2016) can be calibrated from a large survey of noisy time series. Besides some of the literature mentioned earlier (Nilsson et al. 2018; Covino et al. 2019; Yang et al. 2021b), in a sample of 38 bright AGNs, Ashton & Middleton (2021) analysed the X-ray energy-resolved light curves and reported QPO candidates in six sources after accounting for the underlying broad-band noise. Decade-long *Fermi*-LAT observations of 20 blazars were utilized to search for periodic modulations, and year-time-scale QPOs were detected in 5 sources against the red noise (Bhatta & Dhital 2020). However, it is unreliable to state that there is a high proportion of QPO signals that existed in light curves of AGNs, due to the selection effects associated with blazar samples. In a realistic large sample analysis, Peñil et al. (2020) systematically studied γ-ray periodicity in 2274 AGNs by means of an automatic periodicity-search pipeline composed of 10 algorithms, and found 11 sources showing periodicity at a high confidence level.

Nevertheless, in-depth and systematic studies of a large sample of sources or individual sources can help in understanding the periodic behaviour of AGNs. PKS 1510−089 is among the few blazars that have been suggested to have periodic or quasi-periodic variations. In optical band, periodic deep flux minima of 1.84 ± 0.1 yr and the corresponding half-period of 0.92 ± 0.03 yr had been observed (e.g. Xie et al. 2002, 2004), which is in agreement with quasi-periodic outbursts of 1.82 ± 0.12 and 0.92 ± 0.04 yr detected in Metsähovi light curves at 22 and 37 GHz from 1990 to 2005 (Xie et al. 2008). However, Nilsson et al. (2018) did not find any significant QPO in the long-term optical *R*-band light curve. In *Fermi* γ-ray light curve of PKS 1510−089, Sandrinelli et al. (2016) reported a significant QPO of 115 d that may be inter-related with strong QPOs detected in their optical light curves. In one recent multiwavelength study of this source, Castignani et al. (2017) concluded that there is no strong evidence for QPOs in the X-ray and γ-ray light curves at few-year time-scales, although their γ-ray LS periodogram shows a peak at 115 d that is formally in agreement with the finding in Sandrinelli et al. (2016).

In most cases, QPOs claimed in blazar light curves on diverse time-scales seemed to be transient phenomena (e.g. Bhatta 2017; Zhou et al. 2018; Sarkar et al. 2021; Li et al. 2021a; Roy et al. 2022). As for PKS 1510−089, prominent QPOs of about 1080 d with high confidence (>4σ) in University of Michigan Radio Astronomical Observatory (UMRAO) radio light curves had been reported by Li et al. (2021a), who underlined the existence of a transient signature in their detected QPO and the caution of earlier works with no consideration of statistical significance and red noise influence. Most recently, Roy et al. (2022) found two transient QPOs in the *Fermi*-LAT light curve of this source: one is 3.6 d at ∼3σ significance level that lasted for five cycles, and another is 92 d at ∼7σ that lasted for seven cycles. In any case, either transient nature of possible 1080-d periodicity detected in this source or reappearance of other transient QPOs mentioned earlier will further constrain the physical process of the underlying blazar QPO phenomena.

A recent systematic summary for periodic driving mechanisms can be found in Bhatta & Dhital (2020) and Bhatta (2021), who summarized the origin of the QPOs into different scenarios: Keplerian motion in the SMBBH systems, instabilities of the accretion discs around the central engines, and helical motion of emission regions in jets. Generally, QPOs with daily or monthly time-scales can be attributed to the physical models associated with accretion disc fluctuations and disc–jet coupling scenarios such as oscillation modes of the surrounding accretion disc, instabilities in the disc, and orbital rotation of a hotspot around the central black hole (e.g. Pihajoki, Valtonen & Ciprini 2013; Bhatta 2017; Gupta et al. 2019; Kushwaha et al. 2020; Li et al. 2021b, and references therein). Roy et al. (2022) attributed their detected 3.6-d QPO to enhancements by magnetic reconnection events at quasi-equispaced magnetic islands, and their 92-d QPO to a plasma blob moving helically inside a curved jet. However, quasi-periodic signals with time-scales of a few months cannot be derived from our weekly averaged data. Here, we may explain the observed radio QPO of

1330 d as the results of Keplerian motion in the SMBBH system and modulation induced by the Lense–Thirring precession of the disc.

For year-long QPOs, quasi-oscillation periods arising out of the SMBBH systems have been intriguingly discussed. The observed time-scales reflecting the binary system's orbital periodicity are induced by the secondary black hole, and given by $P = 2\pi a^{3/2}\,[G(m+M)]^{-1/2}$, where M and m represent the masses of the primary and secondary black holes, respectively, a is the length of the semimajor axis of the elliptic orbit, and G is the gravitational constant. Assuming a mass ratio $m/M = 0.01$ and the mass of the central black hole (M) of $3 \times 10^8\,\mathrm{M}_\odot$ (Castignani et al. 2017), the separation between the black holes can be estimated as ∼0.0077 pc or ∼270 gravitational radius (r_g). Here, the intrinsic period at the local galaxy would be $1330/(1+z) \approx 977$ d. Due to the emission of low-frequency gravitational wave (GW), such a binary system can undergo orbital decay with a decay time-scale (see Peters 1964; Bhatta & Dhital 2020)

$$\tau = 3.05 \times 10^{-6} \left(\frac{M}{10^9\,\mathrm{M}_\odot}\right)^{-3} \left(\frac{a}{r_\mathrm{g}}\right)^4 \approx 5.70 \times 10^5\ \mathrm{yr}, \qquad (9)$$

corresponding to the GW emission of frequency 5.56×10^{-5} nHz. However, currently available missions do not allow us to detect the coalescence of this binary system.

The quasi-periodic modulation might also be related to the precession period of the blazar jet due to a number of effects, such as Lense–Thirring or spin–stellar disc interaction (see Sobacchi et al. 2017, and references therein). In the strong gravitational field of a rotating central SMBH, the nearby inertial frames can be warped due to the frame dragging effect. Such twisting can result in the nodal precession on tilted orbits around the SMBH spin, known as the Lense–Thirring precession (e.g. Stella & Vietri 1998; Fragile & Meier 2009; Motta et al. 2011). In this case, the wiggling of the jet can lead to quasi-periodic contributions to the observational variabilities. The Lense–Thirring scenario has been widely considered for QPOs detected in stellar-mass black hole systems (e.g. Ingram & Motta 2019), and has been used to explain the quasi-periodic signals found in blazars (e.g. King et al. 2013; Sandrinelli et al. 2016; Sobacchi et al. 2017; Liska et al. 2018; Bhatta & Dhital 2020). The Lense–Thirring precession period is given by

$$P_\mathrm{LT} = \frac{8\pi G M}{c^3 a} \left(\frac{r}{r_\mathrm{g}}\right)^3, \qquad (10)$$

where a, M, and r are the SMBH spin parameter, mass of the black hole, and the radial distance from the black hole system barycentre, respectively. For the QPO of 1330 ± 55 d, and mass of the central black hole $M = 3 \times 10^8\,\mathrm{M}_\odot$ (Castignani et al. 2017), the radius of the inner precessing region is estimated to be $\sim 13 r_\mathrm{g}$ for a dimensionless spin parameter of $a = 0.9$. Due to the warped accretion discs, the precession of the disc can result in a jet precession, therefore producing periodic modulations. As for the transient QPO of 1080 d found in the 4.8-, 8-, and 14.5-GHz UMRAO light curves (Li et al. 2021a), it is difficult to verify whether a Lens–Thirring model can produce close QPO components in nearby wavebands under the present conditions. For a transient QPO, a physical process involving stochastic behaviours (e.g. blobs evolving in jets) would be a better choice.

Although some periodic results have been carried out in systematic studies for individual sources or large samples of sources with different kinds of methods, the search and explanation for possible QPO components in multiwavelength light curves of AGNs is still challenging, and the periodic behaviour related to the astrophysical nature of AGNs needs to be treated with caution. In any case, the possible QPO of 1330 ± 55 d observed in this work presents another interesting case among AGN QPO phenomena and deserves further consideration, especially the false positive rate in large samples of noisy time series, the combination of Fourier-like and non-Fourier methods, and multiwavelength observations covering longer time spans.

ACKNOWLEDGEMENTS

We sincerely thank the anonymous reviewer for constructive comments and suggestions that greatly improved this manuscript. This publication makes use of data obtained from FSSC, and Metsähovi Radio Observatory, operated by Aalto University in Finland. Light-curve simulation and significance estimation were performed on the Key Laboratory of High Density Computing, Zhaotong University. X-PL acknowledges the support from the 'Yunnan Revitalization Talent Support Program' of Yunnan Province, China. This work was supported by the National Natural Science Foundation of China (Grant No. 11903028).

DATA AVAILABILITY

The *Fermi*-LAT data used in this article are available in the LAT data server at https://fermi.gsfc.nasa.gov/ssc/data/access/. The radio 37-GHz observations underlying this article were provided by the Metsähovi monitoring program. For data requests and more details, contact agn-metsahovi@aalto.fi.

REFERENCES

Abdo A. A. et al., 2009, ApJS, 183, 46
Abdollahi S. et al., 2020, ApJS, 247, 33
Ackermann M. et al., 2015, ApJ, 813, L41
Ait Benkhali F., Hofmann W., Rieger F. M., Chakraborty N., 2020, A&A, 634, A120
Akaike H., 1974, IEEE Trans. Autom. Control, 19, 716
Aleksić J. et al., 2014, A&A, 569, A46
An T., Baan W. A., Wang J.-Y., Wang Y., Hong X.-Y., 2013, MNRAS, 434, 3487
Ashton D. I., Middleton M. J., 2021, MNRAS, 501, 5478
Beaklini P. P. B., Dominici T. P., Abraham Z., 2017, A&A, 606, A87
Bhatta G., 2017, ApJ, 847, 7
Bhatta G., 2021, ApJ, 923, 7
Bhatta G., Dhital N., 2020, ApJ, 891, 120
Bhatta G. et al., 2016, ApJ, 832, 47
Bonning E. et al., 2012, ApJ, 756, 13
Burke C. J. et al., 2021, Science, 373, 789
Caproni A., Abraham Z., Motter J. C., Monteiro H., 2017, ApJ, 851, L39
Castignani G. et al., 2017, A&A, 601, A30
Chatterjee R. et al., 2008, ApJ, 689, 79
Connolly S. D., 2015, preprint (arXiv:1503.06676)
Costamante L., Cutini S., Tosti G., Antolini E., Tramacere A., 2018, MNRAS, 477, 4749
Covino S., Sandrinelli A., Treves A., 2019, MNRAS, 482, 1270
Covino S., Landoni M., Sandrinelli A., Treves A., 2020, ApJ, 895, 122
Edelson R., Turner T. J., Pounds K., Vaughan S., Markowitz A., Marshall H., Dobbie P., Warwick R., 2002, ApJ, 568, 610
Emmanoulopoulos D., McHardy I. M., Papadakis I. E., 2013, MNRAS, 433, 907
Foreman-Mackey D., Agol E., Ambikasaran S., Angus R., 2017, AJ, 154, 220
Foster G., 1996, AJ, 112, 1709
Fragile P. C., Meier D. L., 2009, ApJ, 693, 771

Goyal A. et al., 2018, ApJ, 863, 175
Goyal A. et al., 2022, ApJ, 927, 214
Graham M. J. et al., 2015, Nature, 518, 74
Gupta A. C., Srivastava A. K., Wiita P. J., 2009, ApJ, 690, 216
Gupta A. C., Tripathi A., Wiita P. J., Kushwaha P., Zhang Z., Bambi C., 2019, MNRAS, 484, 5785
Hartman R. C. et al., 1999, ApJS, 123, 79
H.E.S.S. Collaboration, 2021, A&A, 648, A23
Hovatta T., Tornikoski M., Lainela M., Lehto H. J., Valtaoja E., Torniainen I., Aller M. F., Aller H. D., 2007, A&A, 469, 899
Ingram A. R., Motta S. E., 2019, New Astron. Rev., 85, 101524
Kaur N., Sameer, Baliyan K. S., Ganesh S., 2017, MNRAS, 469, 2305
Kelly B. C., Bechtold J., Siemiginowska A., 2009, ApJ, 698, 895
Kelly B. C., Becker A. C., Sobolewska M., Siemiginowska A., Uttley P., 2014, ApJ, 788, 33
King O. G. et al., 2013, MNRAS, 436, L114
Kushwaha P., Sinha A., Misra R., Singh K. P., de Gouveia Dal Pino E. M., 2017, ApJ, 849, 138
Kushwaha P., Sarkar A., Gupta A. C., Tripathi A., Wiita P. J., 2020, MNRAS, 499, 653
Lachowicz P., Gupta A. C., Gaur H., Wiita P. J., 2009, A&A, 506, L17
Lähteenmäki A., Järvelä E., Ramakrishnan V., Tornikoski M., Tammi J., Vera R. J. C., Chamani W., 2018, A&A, 614, L1
Li X.-P., Luo Y.-H., Yang H.-Y., Yang C., Cai Y., Yang H.-T., 2017, ApJ, 847, 8
Li X.-P., Luo Y.-H., Yang H.-Y., Yang C., Cai Y., Yang H.-T., Zhou L., Shan Y.-Q., 2018, Ap&SS, 363, 169
Li X.-P., Zhao L., Yan Y., Wang L.-S., Yang H.-T., Cai Y., Luo Y.-H., 2021a, J. Astrophys. Astron., 42, 92
Li X.-P., Cai Y., Yang H.-T., Luo Y.-H., Yan Y., He J.-Y., Wang L.-S., 2021b, MNRAS, 506, 1540
Liska M., Hesp C., Tchekhovskoy A., Ingram A., van der Klis M., Markoff S., 2018, MNRAS, 474, L81
Lomb N. R., 1976, Ap&SS, 39, 447
MAGIC Collaboration, 2018, A&A, 619, A45
Marscher A. P. et al., 2010, ApJ, 710, L126
Massaro E., Perri M., Giommi P., Nesci R., 2004, A&A, 413, 489
Mattox J. R. et al., 1996, ApJ, 461, 396
Max-Moerbeck W., Richards J. L., Hovatta T., Pavlidou V., Pearson T. J., Readhead A. C. S., 2014, MNRAS, 445, 437
Mohan P., Mangalam A., 2015, ApJ, 805, 91
Moreno J., Vogeley M. S., Richards G. T., Yu W., 2019, PASP, 131, 063001
Motta S., Muñoz-Darias T., Casella P., Belloni T., Homan J., 2011, MNRAS, 418, 2292
Nilsson K. et al., 2018, A&A, 620, A185
Orienti M. et al., 2013, MNRAS, 428, 2418
Otero-Santos J. et al., 2020, MNRAS, 492, 5524
Peñil P. et al., 2020, ApJ, 896, 134
Peters P. C., 1964, Phys. Rev., 136, 1224
Pihajoki P., Valtonen M., Ciprini S., 2013, MNRAS, 434, 3122
Press W. H., 1978, Comments Astrophys., 7, 103
Rajput B., Stalin C. S., Sahayanathan S., 2020, MNRAS, 498, 5128
Ramakrishnan V., Hovatta T., Nieppola E., Tornikoski M., Lähteenmäki A., Valtaoja E., 2015, MNRAS, 452, 1280
Ren G.-W., Ding N., Zhang X., Xue R., Zhang H.-J., Xiong D.-R., Li F.-T., Li H., 2021, MNRAS, 506, 3791
Roy N., Chatterjee R., Joshi M., Ghosh A., 2019, MNRAS, 482, 743
Roy A., Sarkar A., Chatterjee A., Gupta A. C., Chitnis V., Wiita P. J., 2022, MNRAS, 510, 3641
Ryan J. L., Siemiginowska A., Sobolewska M. A., Grindlay J., 2019, ApJ, 885, 12
Saito S., Stawarz Ł., Tanaka Y. T., Takahashi T., Madejski G., D'Ammando F., 2013, ApJ, 766, L11
Sandrinelli A., Covino S., Dotti M., Treves A., 2016, AJ, 151, 54
Sarkar A. et al., 2019, ApJ, 887, 185
Sarkar A., Kushwaha P., Gupta A. C., Chitnis V. R., Wiita P. J., 2020, A&A, 642, A129
Sarkar A., Gupta A. C., Chitnis V. R., Wiita P. J., 2021, MNRAS, 501, 50
Scargle J. D., 1982, ApJ, 263, 835
Shah Z., Mankuzhiyil N., Sinha A., Misra R., Sahayanathan S., Iqbal N., 2018, Res. Astron. Astrophys., 18, 141
Sobacchi E., Sormani M. C., Stamerra A., 2017, MNRAS, 465, 161
Sobolewska M. A., Siemiginowska A., Kelly B. C., Nalewajko K., 2014, ApJ, 786, 143
Stella L., Vietri M., 1998, ApJ, 492, L59
Tanner A. M., Bechtold J., Walker C. E., Black J. H., Cutri R. M., 1996, AJ, 112, 62
Teraesranta H. et al., 1998, A&AS, 132, 305
Timmer J., Koenig M., 1995, A&A, 300, 707
Tripathi A., Gupta A. C., Aller M. F., Wiita P. J., Bambi C., Aller H., Gu M., 2021, MNRAS, 501, 5997
Urry C. M., Padovani P., 1995, PASP, 107, 803
Uttley P., McHardy I. M., Papadakis I. E., 2002, MNRAS, 332, 231
Uttley P., McHardy I. M., Vaughan S., 2005, MNRAS, 359, 345
Vaughan S., 2005, A&A, 431, 391
Vaughan S., 2012, Phil. Trans. R. Soc. London Ser. A, 371, 20110549
Vaughan S., Uttley P., Markowitz A. G., Huppenkothen D., Middleton M. J., Alston W. N., Scargle J. D., Farr W. M., 2016, MNRAS, 461, 3145
Virtanen P. et al., 2020, Nat. Methods, 17, 261
Wang J.-Y., An T., Baan W. A., Lu X.-L., 2014, MNRAS, 443, 58
Xie G. Z., Liang E. W., Zhou S. B., Li K. H., Dai B. Z., Ma L., 2002, MNRAS, 334, 459
Xie G. Z., Zhou S. B., Li K. H., Dai H., Chen L. E., Ma L., 2004, MNRAS, 348, 831
Xie G. Z., Yi T. F., Li H. Z., Zhou S. B., Chen L. E., 2008, AJ, 135, 2212
Yang J., Cao G., Zhou B., Qin L., 2021a, PASP, 133, 024101
Yang S., Yan D., Zhang P., Dai B., Zhang L., 2021b, ApJ, 907, 105
Zacharias M. et al., 2019, Galaxies, 7, 41
Zhang H., Yan D., Zhang P., Yang S., Zhang L., 2021, ApJ, 919, 58
Zhang P.-f., Yan D.-h., Liao N.-h., Wang J.-c., 2017a, ApJ, 835, 260
Zhang P.-F., Yan D.-H., Zhou J.-N., Fan Y.-Z., Wang J.-C., Zhang L., 2017b, ApJ, 845, 82
Zheng Y. G., Yang C. Y., Zhang L., Wang J. C., 2017, ApJS, 228, 1
Zheng Y. G., Kang S. J., Yang C. Y., Bai J. M., 2019, ApJ, 873, 7
Zhou J., Wang Z., Chen L., Wiita P. J., Vadakkumthani J., Morrell N., Zhang P., Zhang J., 2018, Nat. Commun., 9, 4599
Zhou R. X., Zheng Y. G., Zhu K. R., Kang S. J., 2021, ApJ, 915, 59

This paper has been typeset from a TEX/LATEX file prepared by the author.